

Roughness-induced magnetic decoupling at organic-inorganic interface

Hiroki Ono,¹ Yoshitaka Umeda,¹ Kaito Yoshida,¹ Kenzaburo Tsutsui,¹ Kohei Yamamoto,² Osamu Ishiyama,² Hiroshi Iwayama,² Eiken Nakamura,² Toshihiko Yokoyama,² Masaki Mizuguchi,^{1,3} and Toshio Miyamachi^{1,3,*}

¹*Graduate School of Engineering and School of Engineering,
Nagoya University, Furo-cho, Chikusa-ku, Nagoya, Aichi 464-8603, Japan*

²*Department of Materials Molecular Science, Institute for Molecular Science, Okazaki 444-8585, Japan*

³*Institute of Materials and Systems for Sustainability (IMaSS),
Nagoya University, Furo-cho, Chikusa-ku, Nagoya, Aichi 464-8601, Japan*

(Dated: May 24, 2023)

We have investigated structural, electronic and magnetic properties of H₂Pc on Fe₂N/Fe using low-energy electron diffraction and soft x-ray absorption spectroscopy/x-ray magnetic circular dichroism. Element specific magnetization curves reveal that the magnetic coupling with H₂Pc enhances the perpendicular magnetic anisotropy of Fe₂N/Fe at the H₂Pc coverage of 1 molecular layer. However, adding two and three molecular layers of H₂Pc reverts the shape of magnetization curve back to the initial state before H₂Pc deposition. We successfully link appearance and disappearance of the magnetic coupling at the H₂Pc-Fe₂N/Fe interface with the change of hybridization strength at N sites accompanied by the increase in the H₂Pc coverage.

PACS numbers:

Organic materials are expected to be useful to spintronics devices because of long spin lifetime derived from their intrinsic weak spin-orbit coupling. Especially, an organic-inorganic hybrid interface has attracted much attention due to its controllable interfacial spin states via electronic hybridization¹. Recent spin-dependent electron transport measurements reveal the importance of not only electronic hybridization but also local structures at the organic-inorganic interface on the emergence of novel spin functionalities^{2,3}. In the case of organic molecules on a magnetic substrate, light elements such as H, C, N, O, which constitute an organic molecule, can magnetize via magnetic coupling with the substrate, playing an important role in characterizing magnetic properties of the whole system^{4,5}. Since the hybridization strength considerably depends on molecular adsorption structure, precise control of the magnetic coupling at the single molecule level is required. However, an experimental study based on the hybridization of light elements in an organic molecule with magnetic substrate has been rarely done.

Here we investigate the magnetic coupling of organic-inorganic interface consisting of metal-free phthalocyanine (H₂Pc) molecules and a bilayer γ' -Fe₄N (Fe₂N/Fe) on Cu(001) (see Fig.1 (a)). In contrast to imperfect layer-by-layer growth of pristine Fe atomic layers on Cu(001)⁶, Fe₂N/Fe grows with atomically flat and homogeneous surface due to its high lateral lattice stability^{7,8}. This allows to selectively extract the impact of molecular adsorption geometry on the magnetic coupling. H₂Pc is a prototypical planar molecule, and chosen as an organic molecule in this work since the efficient hybridization with a magnetic substrate is expected due to its preferential π^* -conjugated configuration⁹. In addition, An H₂Pc molecule consists only of H, C, N, and thus suitable to investigate the magnetic coupling with Fe₂N/Fe in terms of light elements. The results demonstrate that

the formation of the magnetic coupling between H₂Pc and Fe₂N/Fe can clearly appear as the increase in the hybridization strength at N sites.

H₂Pc/Fe₂N/Fe hybrid thin films were grown on Cu(001) in ultrahigh vacuum (UHV) with the base pressure better than 2×10^{-10} Torr. A cyclic process of Ar⁺ ion sputtering and annealing at ~ 700 K of Cu(001) was first conducted to prepare atomically flat and clean substrate surface. Fe₂N/Fe was then fabricated by depositing Fe using an electron-bombardment-type evaporator onto N⁺ ion bombarded Cu(001) with an energy of 0.5 keV, and by subsequent annealing at ~ 600 K. Finally, H₂Pc molecules were deposited on Fe₂N/Fe/Cu(001) at 600 K in the base pressure better than 5×10^{-10} Torr, while keeping the substrate at room temperature. Surface structures, element-specific electronic and magnetic properties of H₂Pc/Fe₂N/Fe were investigated by low-energy electron diffraction (LEED) and soft x-ray absorption spectroscopy/x-ray magnetic circular dichroism (XAS/XMCD). XAS/XMCD measurements were performed at BL 4B of UVSOR-III in a total electron yield mode at 8 K and $B = 0 - \pm 5$ T in the base pressure of $\sim 1 \times 10^{-10}$ Torr¹⁰. XAS spectra were recorded at θ between 0° and 75°, which is the incident x-ray angle with respect to the surface normal. The XMCD spectrum was defined as $\mu_+ - \mu_-$ recorded at the normal (NI: $\theta = 0^\circ$) and the grazing (GI: $\theta = 55^\circ$) geometries. Note that μ_+ and μ_- were the XAS spectra with the photon helicity parallel and antiparallel to the magnetic field direction, respectively. The circular polarization of the x-ray was set to $\sim 65\%$. The coverages of Fe₂N/Fe and H₂Pc were determined by the quartz-crystal microbalance (QCM) and XAS edge jump^{7,11}.

Structural properties of H₂Pc/Fe₂N/Fe hybrid thin films are characterized by XAS and LEED. Figure 1(b) displays XAS spectra of Fe and Cu L edges of Fe₂N/Fe on Cu(001). The Fe coverage can be evaluated with sub-

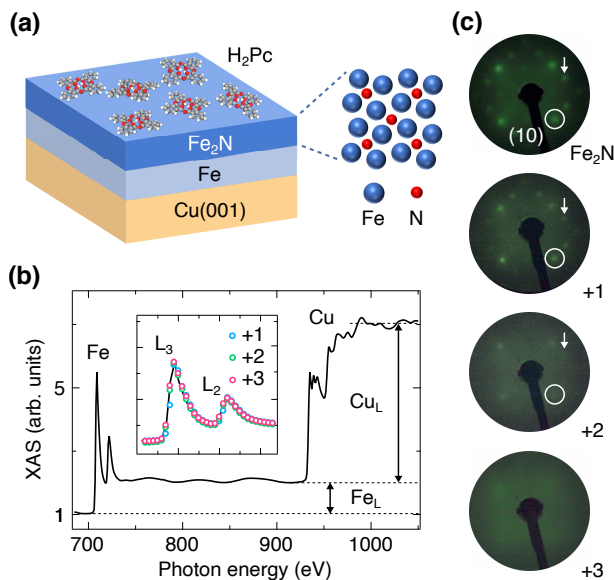


FIG. 1: (a) Schematics of H₂Pc/Fe₂N/Fe hybrid thin films (left panel) and the p4gm(2×2) reconstruction in the Fe₂N layer (right panel). Blue and red spheres represent Fe and N atoms, respectively. (b) Fe and Cu L_{2,3} XAS spectra of Fe₂N/Fe on Cu(001) recorded in the NI geometry. The inset displays Fe L_{2,3} XAS spectra of bare Fe₂N/Fe (solid line), and with 1 (blue), 2 (green) and 3 (pink) ML H₂Pc, respectively. (c) LEED patterns of bare Fe₂N/Fe on Cu(001), and with 1, 2 and 3 ML H₂Pc (from top to bottom). The incident energy is set to 130 eV. Circles and arrows represent LEED spots derived from the p(1×1) lattice and p4gm(2×2) superlattice.

monolayer accuracy from the ratio of the XAS edge jump of Fe to that of Cu (Fe_L/Cu_L). Considering Fe_L/Cu_L of ~ 0.1 as the Fe coverage of a single atomic layer^{7,12,13}, Fe_L/Cu_L of ~ 0.2 in this work ensures controlled Fe deposition by QCM to fabricate Fe₂N/Fe. We further confirm that the shape and relative intensity of L₃ and L₂ peaks of Fe XAS spectrum are almost unchanged after deposition of 1, 2 and 3 molecular layer (ML) of H₂Pc as shown in the inset of Fig. 1(b). This indicates that the structural transition from Fe₂N/Fe to Fe/Fe assisted by the nitrogen surfactant effect^{7,12,13} is absent and the Fe₂N lattice is preserved after H₂Pc deposition since magnetic moments derived from Fe 3d electronic states distributed near the Fermi energy (E_F) are quite different between Fe₂N/Fe and Fe/Fe on Cu(001)^{7,14}.

Figure 1(c) displays a series of LEED patterns of Fe₂N/Fe on Cu(001) with H₂Pc overlayers (0, 1, 2 and 3 ML). The incident electron energy of 130 eV leads to the LEED probing depth of at most several atomic layers. The LEED pattern of bare Fe₂N/Fe shows the p4gm(2×2) reconstructed structure (see right panel of Fig.1(a)), which is characteristic of the topmost Fe₂N layer as previously reported^{7,11,15}. We find that the p4gm(2×2) LEED pattern is observed after deposition of 1ML H₂Pc. The appearance of the p4gm(2×2) LEED pattern is a clear evidence of the existence of the Fe₂N

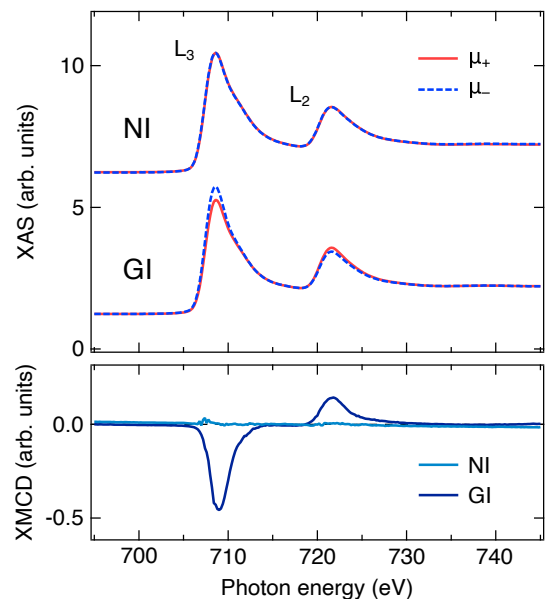


FIG. 2: Fe L_{2,3} remanent XAS and XMCD spectra of Fe₂N/Fe on Cu(001) recorded in the NI and GI geometries. After application of magnetic field up to ± 5 T, the XAS spectra are recorded at remanence conditions ($\pm 5 \rightarrow 0$ T). All the XAS spectra are normalized by the edge jump intensity.

layer underneath 1 ML H₂Pc, and is in line with observed H₂Pc coverage dependence of the Fe XAS spectra as shown in the inset of Fig. 1(b). With increasing the coverage of H₂Pc to 2 ML, LEED spots derived from the p4gm(2×2) superlattice in addition to the p(1×1) lattice are still recognizable. At the coverage of 3 ML H₂Pc, no clear LEED spot is observed. It is important to note that no additional superstructure spots derived from H₂Pc are observed throughout LEED observations in the energy range from 14 to 150 eV. In addition, the LEED background intensity is significantly enhanced as the coverage of H₂Pc increases. The above results provide the information on the growth of H₂Pc/Fe₂N/Fe hybrid thin films; H₂Pc molecules stack on Fe₂N/Fe in a disordered manner and the roughness of surface and interface considerably increases with increasing the H₂Pc coverage.

For XAS/XMCD measurements, we first check magnetic properties of bare Fe₂N/Fe on Cu(001). Figure 2 displays Fe L edge XAS (μ_+ , μ_-) and XMCD ($\mu_+ - \mu_-$) spectra recorded at remanence conditions in the NI and GI geometries. While the remanent XMCD signal is observed in the GI geometry, that is almost negligible in the NI geometry, which clearly reveals the strong in-plane magnetic anisotropy of Fe₂N/Fe on Cu(001). In addition, the spin magnetic moment of Fe₂N/Fe is evaluated to be $1.3 \pm 0.1 \mu_B/\text{atom}$ by XMCD sum rules^{16,17}. These results are in good agreement with the combined experimental and theoretical study of the same system⁷, and thus ensure the high quality of Fe₂N/Fe in this work. Note that the average number of Fe 3d holes, n_{hole} , of

3.22 was used in the sum rule analysis¹⁸.

To investigate details of the magnetic coupling at the interface of H₂Pc and Fe₂N/Fe, we element-specifically measure Fe magnetization curves. Figure 3(a) displays magnetization curves of Fe₂N/Fe with 0, 1, 2, and 3 ML H₂Pc recorded in the GI geometry. A hysteresis loop with saturation magnetization of $\sim \pm 1$ T is observed for bare Fe₂N/Fe, reflecting its in-plane magnetic easy axis. We find that the saturation magnetization of Fe₂N/Fe, which is dominantly attributed to the amplitude of the spin magnetic moment, is almost unchanged after adding H₂Pc overlayers. Indeed, the evaluated spin magnetic moment of Fe₂N/Fe with 1, 2, and 3 ML H₂Pc is $1.2 \pm 0.1 \mu_B/\text{atom}$, which is close to that of bare Fe₂N/Fe ($1.3 \pm 0.1 \mu_B/\text{atom}$). The impacts of H₂Pc overlayers on the Fe magnetization curve can be seen in the coercivity near zero magnetic field. As shown in the inset of Fig. 3(a), a slight decrease in the coercivity is observed for Fe₂N/Fe with 1 ML H₂Pc. However, interestingly, adding 2 ML H₂Pc nearly recovers the coercivity of Fe₂N/Fe to its initial condition, i.e., bare Fe₂N/Fe, and no further changes are recognizable at the H₂Pc coverage of 3 ML. Since the coercivity is determined by various factors such as magnetic anisotropy, formation of magnetic domains, and domain wall pinning¹⁹, it is not straightforward to explain observed H₂Pc coverage dependence only from the Fe magnetization curves recorded in the GI geometry. Therefore, we further investigate its origin from Fe magnetization curves recorded in the NI geometry.

Figure 3(b) displays magnetization curves of Fe₂N/Fe with 0, 1, 2, and 3 ML H₂Pc recorded in the NI geometry. Due to the strong in-plane magnetic anisotropy of Fe₂N/Fe, all the Fe magnetization curves exhibit no remanence. As for the H₂Pc coverage dependence, the Fe magnetization curves show a tendency similar to those recorded in the GI geometry; the shape of the Fe magnetization curve changes only when 1 ML of H₂Pc is deposited on Fe₂N/Fe. Concretely, the Fe magnetization curve becomes steeper with 1 ML H₂Pc. This indicates that adding 1 ML H₂Pc enhances the perpendicular magnetic anisotropy of Fe₂N/Fe, which rationalizes decreased coercivity observed in the GI geometry. Since all H₂Pc molecules are expected to be directly anchored to Fe₂N/Fe at the H₂Pc coverage of 1 ML even though they might be randomly adsorbed on the surface (see Fig.1 (c)), it is reasonable to ascribe the enhancement of the perpendicular magnetic anisotropy of Fe₂N/Fe to the magnetic coupling with H₂Pc. Further changes in the Fe magnetization curve by stacking 2 and 3 ML H₂Pc can be explained in terms of the relationship between the magnetic coupling and local structure at the interface of H₂Pc and Fe₂N/Fe. LEED observations shown in Fig.1 (c) reveal that the surface/interface roughness in this system significantly increases with increasing the H₂Pc coverage. We therefore presume that the second (and third) H₂Pc layer disrupts the molecule-surface bonding of H₂Pc molecules directly anchored to Fe₂N/Fe and inclines them via intermolecular interactions. This

could lead to magnetic decoupling of the first H₂Pc layer from Fe₂N/Fe. Note that similar effects are reported for spin transport measurements of PbPc/Cu/NiFe system³. However, the hybridization between PbPc and Cu inducing a Rashba spin splitting at the interface is relatively robust against the increase in the PbPc coverage, which is in contrast to drastic changes of the degree of the magnetic coupling between H₂Pc and Fe₂N/Fe. This indicates that the degree of the magnetic coupling of organic molecules and inorganic materials with localized d states near the E_F, i.e., Fe 3d states in this work, is quite sensitive to changes of local structure.

To validate the scenario mentioned above, we focus on the H₂Pc coverage dependence of N K-edge XAS. Figure 4(a) displays N K-edge XAS spectra recorded at $\theta = 65^\circ$ for 1, 2, 3 ML H₂Pc on Fe₂N/Fe, and bare Fe₂N/Fe as a reference. As seen for H₂Pc thin films on various substrates^{20,21}, the spectrum consists of two characteristic energy regions; π^* resonances below ~ 404 eV with peaks derived from unoccupied molecular orbitals, LUMO (A), LUMO+1 (B) and LUMO+2 (C) at 398, 400, and 402 eV, and σ^* resonances with broad features at higher energies. Note that the pronounced π^* resonances observed at $\theta = 65^\circ$, where the polarization vector of x-ray is approximately perpendicular to the surface in this study, considerably decrease at $\theta = 15^\circ$ (see SI). This indicates that, in spite of random and disorder stacking as revealed by LEED observations, H₂Pc molecules more or less maintain planar π^* -conjugated configurations with Fe₂N/Fe. In advance to discuss how the magnetic coupling modifies electronic structures of H₂Pc molecules at N sites, we subtract the N K-edge XAS spectrum of bare Fe₂N/Fe as a background from the one of 1, 2, 3 ML H₂Pc on Fe₂N/Fe (see SI), which allows an accurate comparison among them. Figure 4(b) displays π^* resonances in the background-subtracted N K-edge XAS spectra of 1, 2, 3 ML H₂Pc on Fe₂N/Fe. We find that especially peaks B and C are broader for 1 ML H₂Pc, but become sharper for 2 ML H₂Pc. As for 3 ML H₂Pc, the spectral shape is almost identical to that of 2 ML H₂Pc. The magnetic coupling arises as a consequence of electronic hybridization between H₂Pc and Fe₂N/Fe. The hybridization of molecular orbitals with substrate can delocalize LUMO²², resulting in the broadening of peaks in the N K-edge XAS spectrum²⁰. Thus, broad peaks observed for 1 ML H₂Pc is a clear signature of the efficient hybridization, i.e., magnetic coupling with Fe₂N/Fe. Furthermore, narrowing of the peak width with increasing the H₂Pc coverage to 2, and 3 ML is involved in weakening of the hybridization with Fe₂N/Fe, which is consistent with the magnetic decoupling at the interface. These results fully support the conclusions from LEED and XMCD observations. Note that the enhancement of the perpendicular magnetic anisotropy of Fe₂N/Fe with 1 ML H₂Pc is reasonable also in terms of density of states of Fe₂N/Fe and H₂Pc. Among 3d states of Fe₂N on Fe, out-f-plane oriented orbitals, especially $d_{3z^2-r^2}$ and d_{yz} are prominent at the energy range of about 0-3 eV above E_F⁷,

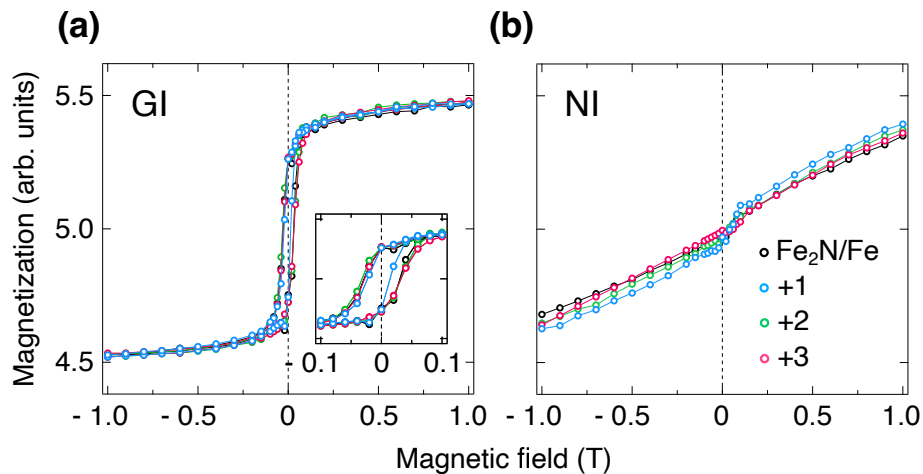


FIG. 3: Magnetization curves of $\text{Fe}_2\text{N}/\text{Fe}$ with 0 (black), 1 (blue), 2 (green) and 3 (pink) ML H_2Pc recorded in the (a) GI and (b) NI geometries, respectively. The L_3 peak intensity in the Fe XAS spectrum normalized by the L_2 one is plotted as a function of magnetic field.

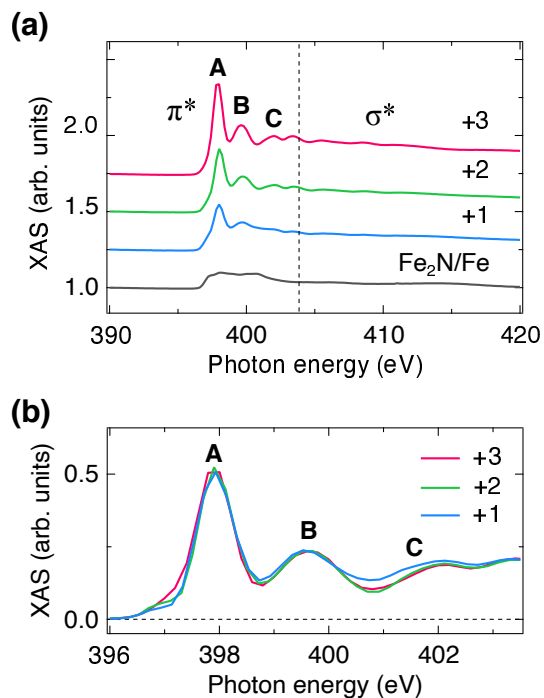


FIG. 4: (a) N K-edge XAS spectra of 0, 1, 2, 3 ML H_2Pc on $\text{Fe}_2\text{N}/\text{Fe}$ (from bottom to top). (b) N K-edge XAS spectra of 1, 2, 3 ML H_2Pc after subtracting $\text{Fe}_2\text{N}/\text{Fe}$ background spectrum. The spectra are normalized by peak intensities and edge jump.

where LUMO (A), LUMO+1 (B) and LUMO+2 (C) of H_2Pc exist. This leads to the broadening of the bandwidth of the out-of-plane 3d orbitals via the hybridization at the interface, which in turn can enhance the out-of-

plane magnetization of $\text{Fe}_2\text{N}/\text{Fe}$ triggered by spin-orbit interaction^{23,24}.

In conclusion, we have investigated the H_2Pc coverage dependence of magnetic properties of $\text{Fe}_2\text{N}/\text{Fe}$ on $\text{Cu}(001)$. The results have revealed that the magnetic coupling enhances the perpendicular magnetic anisotropy of Fe_2N at the H_2Pc coverage of 1 ML, but adding 2 and 3 ML H_2Pc considerably increases surface/interface roughness of the system and accordingly decouples the magnetic interaction. We have additionally demonstrated the importance of light elements in a organic molecule to elucidate the correlation between structural and electronic/magnetic properties on the level of a single molecule toward utilizing the organic-inorganic interface in molecular spintronics devices.

Acknowledgment

This work was partly supported by JSPS KAKENHI Grant Numbers, JP20H05179, 20K21119, JP21H05016, 22H01957 and JP23H01849. A part of this work was conducted at the BL4B of UVSOR Synchrotron Facility, Institute for Molecular Science supported by Nanotechnology Platform Program <Molecule and Material Synthesis> (JPMXP09S19MS2001b, JPMXP09S19MS2001, JPMXP09S20MS2001, JPMXP09S21MS2001, JPMXP09S21MS2002), and by Advanced Research Infrastructure for Materials and Nanotechnology in Japan (JPMXP1222MS2001, JPMXP1222MS2003) of the Ministry of Education, Culture, Sport, Science and Technology (MEXT), Japan.

-
- * toshio.miyamachi@imass.nagoya-u.ac.jp
- ¹ S. Sanvito, *Nature Phys* **47**, 562–564 (2010).
 - ² H. Nakayama, T. Yamamoto, H. An, K. Tsuda, Y. Einaga, K. Ando, *Sci. Adv.* **4**, eaar3899 (2018).
 - ³ H. Isshiki, K. Kondou, S. Takizawa, K. Shimose, T. Kawabe, E. Minamitani, N. Yamaguchi, F. Ishii, A. Shiotari, Y. Sugimoto, S. Miwa, Y. Otani, *Nano. Lett.* **19**, 7119-7123 (2019).
 - ⁴ F. Djeghloul, F. Ibrahim, M. Cantoni, M. Bowen, L. Joly, S. Boukari, P. Ohresser, F. Bertran, P. Le Fèvre, P. Thakur, F. Scheurer, T. Miyamachi, R. Mattana, P. Senear, A. Jaafar, C. Rinaldi, S. Javaid, J. Arabski, J. -P Kappler, W. Wulfhekel, N. B. Brookes, R. Bertacco, A. Taleb-Ibrahimi, M. Alouani, E. Beaurepaire, W. Weber, *Sci. Rep.* **3**, 1272 (2013).
 - ⁵ S. Gueddida, M. Gruber, T. Miyamachi, E. Beaurepaire, W. Wulfhekel, M. Alouani, *J. Phys. Chem. Lett* **7**, 900-904 (2016).
 - ⁶ A. Biedermann, R. Tscheliessnig, M. Schmid, P. Varga, *Appl. Phys. A* **78**, 807 (2004).
 - ⁷ Y. Takahashi, T. Miyamachi, S. Nakashima, N. Kawamura, Y. Takagi, M. Uozumi, V. N. Antonov, T. Yokoyama, A. Ernst, F. Komori, *Phys. Rev. B* **95**, 224417 (2017).
 - ⁸ T. Hattori, T. Iimori, T. Miyamachi, F. Komori, *Phys. Rev. Materials* **2**, 044003 (2018).
 - ⁹ S. Schmaus, A. Bagrets, Y. Nahas, T. K. Yamada, A. Bork, M. Bowen, E. Beaurepaire, F. Evers, W. Wulfhekel, *Nat. Nanotechnol.* **6**, 185-189 (2011).
 - ¹⁰ T. Nakagawa, Y. Takagi, Y. Matsumoto, T. Yokoyama, *Jpn. J. Appl. Phys.* **47**, 2132 (2008).
 - ¹¹ Y. Takagi, K. Isami, I. Yamamoto, T. Nakagawa, T. Yokoyama, *Phys. Rev. B* **81**, 035422 (2010).
 - ¹² K. Kawaguchi, T. Miyamachi, T. Iimori, Y. Takahashi, T. Hattori, T. Yokoyama, M. Kotsugi, F. Komori, *Phys. Rev. Materials* **4**, 1054403 (2020).
 - ¹³ K. Kawaguchi, T. Miyamachi, T. Gozliniski, T. Iimori, Y. Takahashi, T. Hattori, K. Yamamoto, T. Koitaya, H. Iwayama, O. Ishiyama, E. Nakamura, M. Kotsugi, W. Wulfhekel, T. Yokoyama, F. Komori, *Jpn. J. Appl. Phys* **61**,SL1001 (2022).
 - ¹⁴ H. Abe, K. Amemiya, D. Matsumura, J. Miyawaki, E. O. Sako, T. Otsuki, E. Sakai, T. Ohta, *Phys. Rev. B* **77**, 054409 (2008).
 - ¹⁵ Y. Takahashi, T. Miyamachi, K. Ienaga, N. Kawamura, A. Ernst, F. Komori, *Phys. Rev. Lett.* **116**, 056802 (2016).
 - ¹⁶ B. T. Thole, P. Carra, F. Sette, G. van der Laan, *Phys. Rev. Lett.* **68**, 1943 (1992).
 - ¹⁷ C. T. Chen, Y. U. Idzerda, H.-J. Lin, N. V. Smith, G. Meigs, E. Chaban, G. H. Ho, E. Pellegrin, F. Sette, *Phys. Rev. Lett.* **75**, 152 (1995).
 - ¹⁸ S. Nakashima, T. Miyamachi, Y. Tatetsu, Y. Takahashi, Y. Takagi, Y. Gohda, T. Yokoyama, F. Komori, *Adv. Funct. Mater.* **29**, 1804594 (2019) .
 - ¹⁹ A. Hubert and R. Schäfer, *Magnetic domains* (Springer, Berlin, 1998).
 - ²⁰ E. Annese, J. Fujii, I. Vobornik, G. Panaccione, G. Rossi, *Phys. Rev. B* **84**, 174443 (2011).
 - ²¹ T. M. Willey, M. Bagge-Hansen, J. R. I. Lee, R. Call, L. Landt, T. van Buuren, C. Colesniuc, C. Monton, I. Valmianski, Ivan K. Schuller, *J. Chem. Phys.* **139**, 034701 (2013).
 - ²² T. Miyamachi, M. Gruber, V. Davesne, M. Bowen, S. Boukari, L. Joly, F. Scheurer, G. Rogez, T.K. Yamada, P. Ohresser, E. Beaurepaire, W. Wulfhekel, *Nat. Commun.* **3**, 938 (2012).
 - ²³ J. Stöhr, *J. Magn. Magn. Mater* **200**, 470-497 (1999).
 - ²⁴ P. Bruno, *Phys. Rev. B* **39**, 865 (1989).